ACS APPLIED MATERIALS & INTERFACES

Research Article

www.acsami.org

Robust, Uniform, and Highly Emissive Quantum Dot–Polymer Films and Patterns Using Thiol–Ene Chemistry

Marcus J. Smith,[†,‡] Sidney T. Malak,[†] Jaehan Jung,[†,§] Young Jun Yoon,[†] Chun Hao Lin,[†] Sunghan Kim,[†] Kyung Min Lee,[‡] Ruilong Ma,[†] Timothy J. White,[‡] Timothy J. Bunning,[‡] Zhiqun Lin,[†] and Vladimir V. Tsukruk*[,†]

[†]School of Materials Science and Engineering, Georgia Institute of Technology, Atlanta, Georgia 30332, United States

[‡]Air Force Research Laboratories, Wright-Patterson Air Force Base, Ohio 45433, United States

[§]Department of Materials Science and Engineering, Hongik University, Sejong 339-701, South Korea

Supporting Information

ABSTRACT: This work demonstrates a facile and versatile method for generating low scattering cross-linked quantum dot (QD)–polymer composite films and patterned highly emissive structures with ultrahigh QD loading, minimal phase separation, and tunable mechanical properties. Uniform QD–polymer films are fabricated using thiol–ene chemistry, in which cross-linked polymer networks are rapidly produced in ambient conditions via fast UV polymerization in bulk to suppress QD aggregation. UV-controlled thiol–ene chemistry limits phase separation through producing highly QD loaded cross-linked composites with loadings above majority of those reported in the literature (<1%) and approaching 30%. As the QD loading is increased, the thiol and ene conversion decreases, resulting in nanocomposites with widely variable and tailorable mechanical properties as a function of UV irradiation time with an elastic modulus decreasing to 1 GPa being characteristic of reinforced elastomeric materials, in contrast to usually observed stiff and brittle materials under these loading conditions. Furthermore, we demonstrate that the thiol–ene chemistry is compatible with soft-imprint lithography, making it possible to pattern highly loaded QD films while preserving the optical properties essential for high gain and low optical loss devices. The versatility of thiol–ene chemistry to produce high-dense QD–polymer films potentially makes it an important technique for polymer-based elastomeric optical metamaterials, where efficient light propagation is critical, like peculiar waveguides, sensors, and optical gain films.

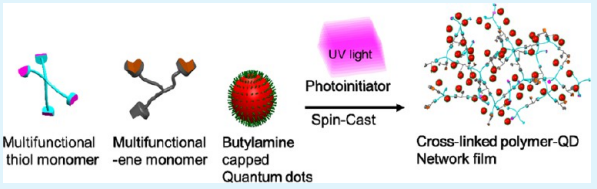

KEYWORDS: *quantum dots, thiol–ene chemistry, polymer nanocomposite, thiol–ene, soft lithography, photoluminescence, quantum yield*

1. INTRODUCTION

Addition of quantum dots (QD) to polymer nanocomposites offers significantly improved function for QD-containing nanocomposites, being able to take advantage of the unique optical and electrical properties of QDs[1] while retaining the versatile bulk mechanical properties of the polymeric matrices.[2] Perfected synthetic techniques have afforded precise control over the QD structure, resulting in superior electronic and optical properties.[3] On the other hand, appropriate monomer selection offers complete control over the underlying polymer matrix and tailorable mechanical properties.[4] The precise engineering of the QD structure allows for increased quantum yield (QY),[5] extended photoluminescence (PL) lifetimes,[6] and attenuated effects from nonradiative decay mechanisms.[7] This has led to the utilization of QDs in areas spanning photovoltaics,[8] solar concentrators,[9] gain media,[10] LEDs,[11] photonics,[12] and next-generation semiconductor lasers.[13] Encapsulation of QDs in a polymer matrix with uniform distribution and suppressed aggregation, while still remaining challenging, has been demonstrated to not only provide added benefits from the bulk properties of the polymer but also improve QD optical properties.[14] Potential applications of these nanocomposites include advanced photonic parity-time (PT) symmetric systems including Bragg reflectors[15] and coupled waveguides,[16] which can display phenomenon like unidirectional invisibility.[17]

Photonic systems, in particular, can benefit greatly from the tunable optical properties of QDs, exhibiting exceptionally high optical gains (a requirement of PT systems) as well as the tailored mechanical properties provided by a polymer matrix, facilitating robust backbones and applicability to a host of planar and nonplanar substrates. Similar systems have been developed for a subfield of photonics, optoelectronic systems, in which encapsulation of conductive wires in elastomeric matrices imparts stability, flexibility, and stretchability.[18] The incorporation of QDs into polymer matrices is a particularly important step because it allows for the fabrication of stable and uniform functional materials with low optical losses, offering

Received: March 8, 2017
Accepted: April 25, 2017
Published: April 25, 2017

DOI: 10.1021/acsami.7b03366
ACS Appl. Mater. Interfaces 2017, 9, 17435–17448

Scheme 1. Schematic Showing (a) Mechanism for Fabrication of NOA-BAQD Composite and (b) Initiation and Propagation of Thiol−Ene Reaction

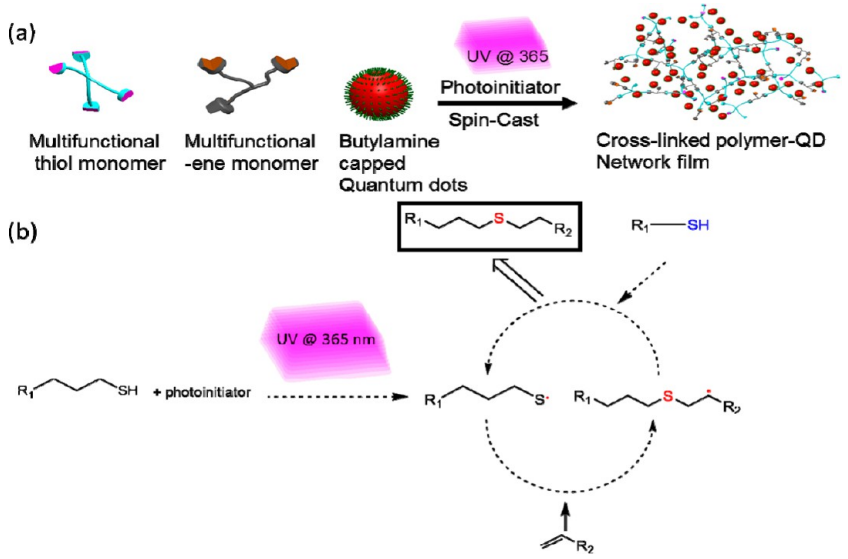

the ability to vary thickness (submicrometers to micrometers), relative ease in processing, and the controlled incorporation of significant quantities of QD gain medium into a matrix for tunable emission strength.

However, the preparation of well dispersed QD−polymer composites is challenging, primarily relating to large-scale phase separation, which results in QD aggregation thus high optical scattering and losses. Recent efforts to develop QD−polymer composites have seen limited success since simple mixing of the two components typically leads to significant QD aggregation and phase separation.[19,20] Wang et al. recently developed microbubble lasers via simple drop-casting of QD−poly(methyl methacrylate) (PMMA) solutions. Loadings above 50% were achieved; however, this methodology is not easily adaptable to patterning, as structures are limited to large shapes.[21] Additionally, although more complex reaction schemes can compromise the valuable properties of the QDs, they have only resulted in inclusion of QDs at very low weight percentages.[22] Specifically, aggregation of QDs typically leads to nonradiative decay mechanisms such as quenching[23] (i.e., Förster resonance energy transfer) as well as optical losses from scattering.[24] In addition, while QD photopatterns of low resolution have been generated utilizing TEM grids as a mask, a clear scalable approach that allows for the fabrication of high-resolution patterns in highly loaded QD composites have not yet been developed.[25] Ehlert et al. demonstrated QD−polymer composites by grafting polymer brushes onto the QD surface and subsequently mixing with like polymers.[26] A proposed method for combating large QD aggregation and phase separation would be the utilization of a fast cross-linking mechanism that takes place on time scales faster than phase separation of relatively large nanoparticles, thereby minimizing the tendency of QDs to phase separate during film formation. Furthermore, it has been suggested that cross-linking during polymerization can reduce aggregation and energy transfer mechanisms, resulting in enhanced emission in comparison to the non-cross-linked counterparts.[27,28]

Thiol−ene photopolymerization has proven to be a versatile reaction that produces cross-linked networks,[29] occurs rapidly, is highly efficient,[30,31] and is largely insensitive to ambient environments.[29,32] Given the weak nature of the sulfur−hydrogen bond, a free-radical initiating species will abstract a hydrogen from the thiol precursor. Subsequently, the thiyl radical will efficiently attack an electron-deficient terminal carbon−carbon double bond, forming a cross-linked network similar to the vulcanization of rubber.[29,32] The cross-link density of thiol−ene photopolymerization can be readily tailored by formulation, enabling tunability of the thermal and mechanical properties of host matrix,[33,34] leading to potentially robust and flexible networks with uniform distribution of components. Moreover, thiol−ene chemistries come in a variety of mixtures depending on the desired properties, including commercially available thiol−ene based optical adhesive mixtures,[35] i.e., Norland Optical Adhesives, which consist of a triene (i.e., 1,3,5-triallyl-1,3,5-triazine-2,4,6(1*H*,3*H*,5*H*)-trione) and a multifunctional mercapto-ester (i.e., pentaerythritol tetrakis(3-mercaptopropionate)), with a urethane-based component, and a benzophenone photoinitiator.[35]

The thiol−ene mechanism has been utilized as a "click" reaction to generate nanoparticle−polymer composites via a "graft from" mechanism where the nanoparticle ligands serve as anchoring sites that participate in the step growth thiol−ene polymerization, producing various cross-linked polymer composites in which the nanoparticles can serve as cross-link sites.[35−38] For instance, Lü et al. grafted thiolated styrene and phenol onto ZnS QDs, followed by a UV-initiated free radical polymerization to form a poly(urethane−methacrylate macromer) composite in which QDs were immobilized in the polymer network, taking advantage of thiol−ene based click chemistry.[39] Similarly, Kim et al. functionalized the surface of QDs with a complex norbornene compound and generated a QD−polymer composite by photopolymerizing the tethered ene with a multifunctional thiol. However, no significant loading was achieved; furthermore, micrometer scale patterns were generated with loading not exceeding 0.2 wt %.[22]

In this work, we explore the photopolymerization of thiol−ene chemistries in the presence of butylamine-capped CdSe/$Cd_{1-x}Zn_xSe_{1-y}S_y$ quantum dots (BAQDs) to generate highly loaded nanocomposite films and patterns with uniform

DOI: 10.1021/acsami.7b03366
ACS Appl. Mater. Interfaces 2017, 9, 17435−17448

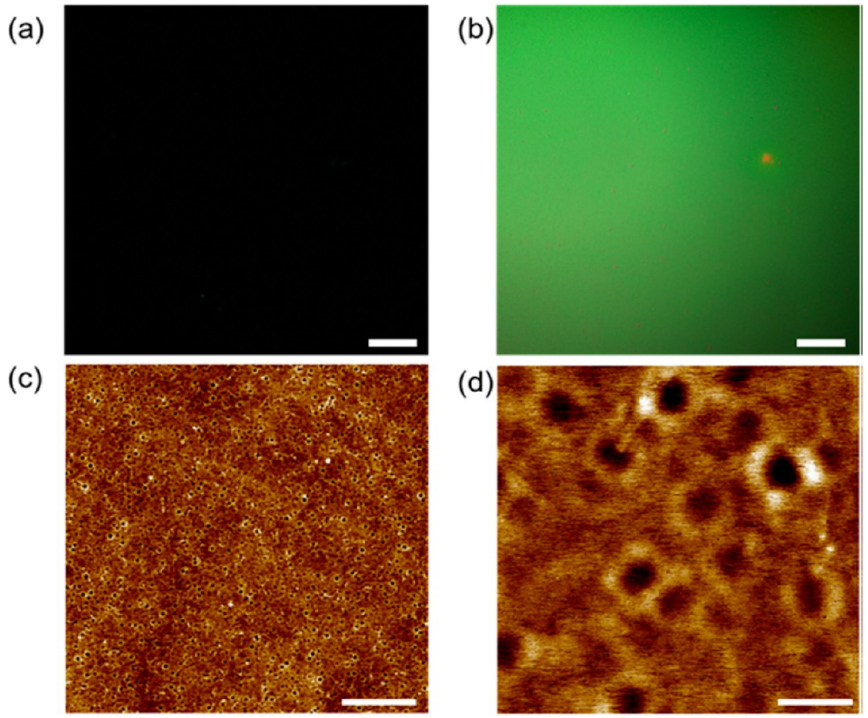

Figure 1. Optical imaging of neat NOA films showing (a) dark field, (b) bright field. Scale bars are 50 μm. AFM images (c) and (d) for neat NOA. Scale bars and height scales for (c) are 10 μm and 7 nm respectively, for (d) 1 μm and 6 nm, respectively.

distribution of QDs and minimal aggregation. We show that the use of cross-linking photopolymerization and QDs with shorter ligands, containing no internal alkene bonds, makes possible the fabrication of homogeneous nanocomposites. These nanocomposites are suitable for optical applications as the polymer network encapsulates the QDs while maintaining strong photoluminescence with minimal optical losses from scattering. While photoluminecense properties typically diminish following ligand exchange, it has been shown in previous work that ligand exchange from oleic acid (OA) to butylamine only lowers the quantum yield from 50% to ∼30%, with some batch to bath variation, maintaining these QDs as strong candidates for high optical gain materials.[40] We suggest that shorter ligands better facilitate thiol−ene cross-linking, as OA possesses an internal alkene, which could potentially interfere with the thiol and−ene cross-linking reaction, as it disrupts the initial stoichiometry. Furthermore, initial films fabricated utilizing oleic acid showed significant amounts of hazing, suggesting large-scale phase separation.

This approach represents a significant departure from previous attempts in that in this work a chemically and mechanically robust network with tunable properties can be fabricated. BA-QDs are encapsulated within the cross-linked polymer network, and phase separation is minimized by utilizing shorter ligands and taking advantage of the rapid photopolymerization process. Furthermore, the addition of QDs, given their typically high quantum yields, alters the UV initiated reaction in such a way that allows for controlled properties as a function of UV irradiation time, facilitating robust, flexible, and highly emissive composites. This approach results in fabricating well-dispersed, highly loaded polymer−QD composite networks which are robust, solvent-resistant, and optically stable for prospective applications in photonics, waveguides, and QD lasers.

2. RESULTS AND DISCUSSION

Norland Optical Adhesive 63 (NOA) utilized in this study consists of a tetrafunctional thiol in a near 1:1 molar ratio with a trifunctional alkene as well as a photoinitiator.[29] Scheme 1 shows the routes which are utilized for fabricating NOA-BAQD polymer composites and intiation and propogation of the thiol−ene reaction. As discussed previously, and illustrated in Scheme 1b, upon irradiation with UV light, a free radical is generated on the sulfur, leading to the thiyl readily attacking carbon−carbon double bonds, preferably terminal ones, causing the polymer reaction to proceed very similar to that of a step growth mechanism.[32] Butylamine was used as the ligand for the BAQDs due to its short chain and the lack of a terminal ene.

Because the amine functionality attaches to the QD surface, the exposed surface chemistry of the particles is a simple alkane, making the ligand highly unlikely to participate in the thiol−ene reaction. The NOA monomer mixture is readily soluble in mildly polar solvents such as chloroform and acetone.[35] Neat NOA films were produced by dissolving a known amount of the adhesive. In chloroform, making a final 1 or 5 wt% NOA solution, and then an aliquot was spin-cast, followed by degassing and UV irradiation. Neat films show minimal optical scattering and have large scale uniformity, as confirmed by dark-field and bright-field optical imaging (Figure 1a,b). Atomic force microscopy (AFM) confirms smooth surface with microroughness $R_q \sim 2$ nm for 5×5 μm^2 surface areas (Figure 1).

A similar approach was used to fabricate a uniform QD−polymer nanocomposite. First, a concentrated solution of BAQDs in chloroform was mixed with a dilute solution (1 or 5 wt %) of NOA in chloroform to produce a NOA-BAQD solution. Subsequently, films were fabricated by spin-casting the concentrated solution of NOA-BAQDs on a silicon wafer, followed by degassing, and immediate exposure to UV light for

DOI: 10.1021/acsami.7b03366
ACS Appl. Mater. Interfaces 2017, 9, 17435−17448

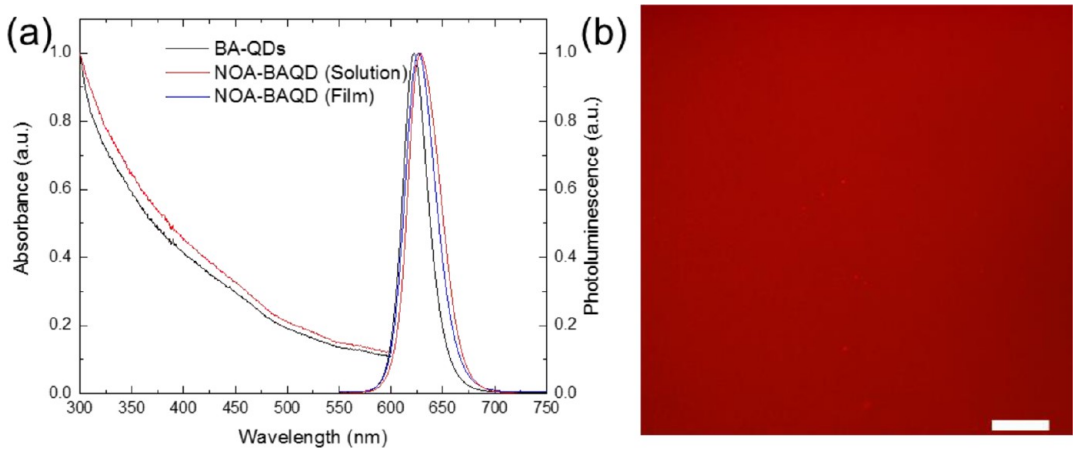

Figure 2. (a) Comparison of absorbance from neat BA-QDs and unpolymerized NOA with BAQDs in solution and photoluminescence from neat BA-QDs in solution, unpolymerized NOA with BAQDs in solution, and NOA-BAQDs in a closed packed polymer film. A slight increase in absorbance and a small redshift as well as slight peak broadening is noticed from pure QD to composite. 50× fluorescence (b) image of a QD-polymer film showing minimal scattering and uniform fluorescence over large areas. Scale bar: 20 μm.

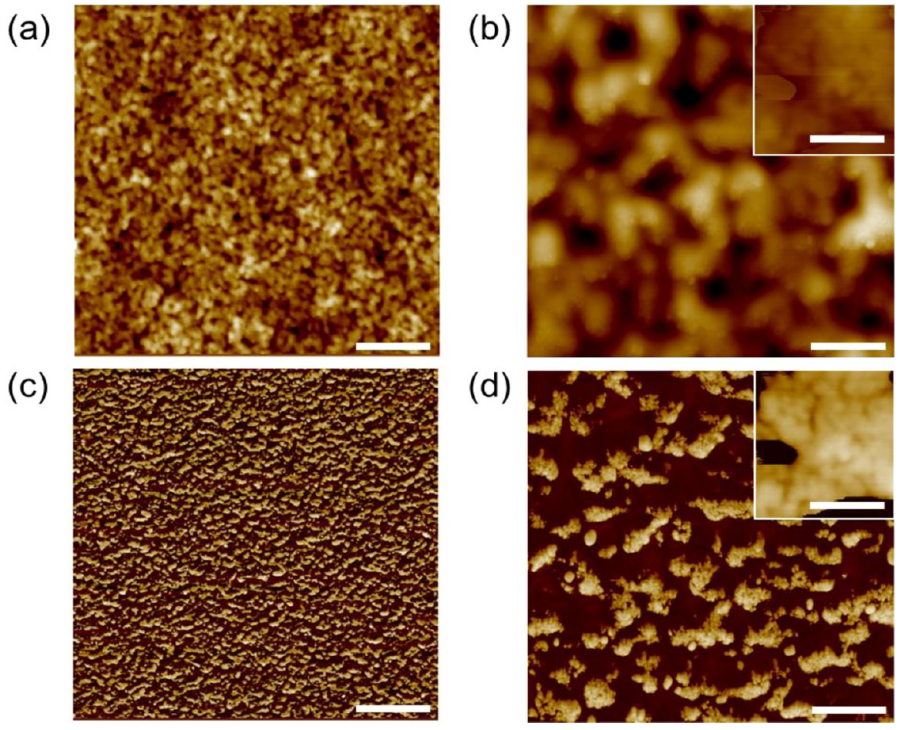

Figure 3. AFM topography (a,b) and phase (c,d) images for highly loaded NOA-BAQD films. Scale bars for (a,c) and (b,d) are 2 μm and 400 nm, respectively. Height scales for (a) and (b) topography images are 100 nm and 80 nm, respectively. Insets show a zoomed in image of NOA-BAQD film showing QD clusters with scale bar of 100 nm.

several minutes. Figure S1 shows TEM images of the BAQDs with average size of 8 nm and AFM images showing surface roughness of below 4 nm for 25 μm^2 surface areas.

The fluorescence emission of the unpolymerized NOA-BAQD solution and composite film is similar to that of the neat BAQDs in solution, with a slight red-shift in the peak position and a slight broadening of the full width at half-maximum (fwhm) (Figure 2a). These changes suggest an energy transfer as caused by a possibly aggregated solution, and a close-packed QD film, as well as optical reabsorption due to the overlap of the absorbance and emission states.[41]

Minimal aggregation in the nanocomposite is further confirmed by uniform dark-field and SEM imaging (Figure S2). Very little scattering is observed in the dark-field image, indicating fine QD−polymer mixing and uniformity without QD aggregation at a submicrometer scale and minimal surface roughness. Furthermore, SEM of the film topology shows some possible aggregation or surface roughness of the polymer composite film. Fluorescence imaging shows uniform emission (intensity and color) as well over large regions of the film, thus confirming the aforementioned conclusion (Figure 2b).

Given the sensitivity of QDs to their environment, the optical properties were further studied to confirm that the close interaction between QD/monomer and QD/polymer did not result in significant alteration of properties (Table S1 and Figure S3). Quantum yield measurements on BAQDs and

DOI: 10.1021/acsami.7b03366
ACS Appl. Mater. Interfaces 2017, 9, 17435−17448

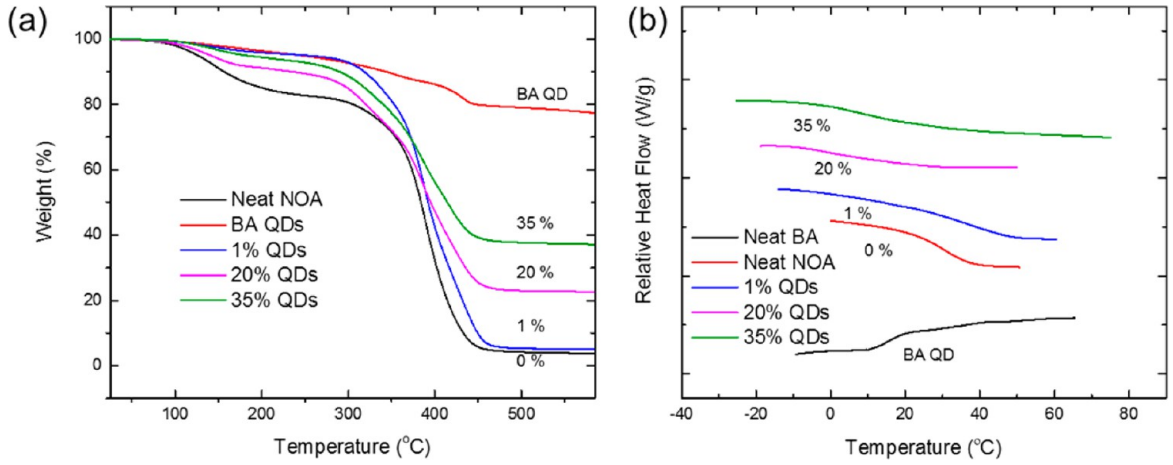

Figure 4. TGA (a) and DSC (b) of neat components and NOA-BAQD composite films. TGA confirms loading, while DSC shows significant reduction in T_g values as loading is increased.

unpolymerized NOA-BAQDs in solution show that no change in QY occurs upon mixing of NOA monomers and BAQDs in solution. Furthermore, comparison of a NOA-BAQD film PL emission relative to a BAQD film shows emission was reduced by half, likely due to volume reduction of QDs present, indicating films still maintain their good optical properties.

Morphology of QD Polymer Films. Topography and phase AFM scans confirm the uniform nature of the QD−polymer surfaces with uniform distribution of nanoscale features (Figure 3). The high-resolution AFM image shows well-dispersed nanoscale domains of random aggregates of about 200 nm in dimension. Higher resolution scans indicate the aggregates are composed of spherical nanoparticles with apparent dimensions below 40 nm due to dilation by the AFM tip (see inset of Figure 3b,d).[42] The RMS roughness of the 500 × 500 nm^2 AFM image is 3.6 nm, indicating very uniform surface nanoscale morphology with minute variation of elevations caused by the presence of the QDs embedded in the polymer matrix.

The heterogeneous nature of the AFM phase image is a clear indication of a multiphase system of nanoscale domains composed of densely packed semiconducting QDs within soft polymer matrix.[43] Phase imaging in AFM can be an effective method for identifying surface properties such as stiffness[43−45] and chemical composition distribution.[43−45] The contrast arises in both the attraction (light tapping) or repulsion (hard tapping) modes between the AFM tip and the surface, resulting in a change of the phase of the oscillating cantilever for different materials components.[46] Though the difference in mechanical properties of the two-phase system is not immediately known, the bright and dark regions shown in the AFM images suggest areas of glassy (bright) and elastomeric (dark) materials, respectively.[47] This difference suggests that the QD aggregates are surrounded by a soft polymer matrix in these *in situ* polymerized nanocomposites. Indeed, for polymer nanoparticle composite systems, Ash et al.[48] suggest the formation of cooperative rearranging regions (CRR) in which nanoadditives can serve as templates for a porous network if there is significant nonwetting at the interface between polymer and additive. We suggest that in our case the aggregation of the QDs disrupts the percolation of the polymer network, resulting in the creation of "nanoscale void regions" in which the polymer surrounding the QD aggregates is compliant. The aggregation observed in this system is nanoscale and uniformly widespread and therefore does not significantly increase optical scattering, disrupt light propagation, or lead to variations in film thickness over the substrate. Furthermore, X-ray diffraction (XRD) shows no phase change and crystal lattice distortions of QDs upon their encapsulation with the NOA polymer (Figure S4).[49] Indeed, all *d*-spacings and peak width remain unchanged with diffuse halo around 20°, indicating amorphous nature of polymer matrix.

Thermal Properties. Next, NOA-BAQD films of varying ratios of BAQD to NOA were analyzed with thermogravimetric analysis (TGA) and differential scanning calorimetry (DSC) to understand how the thermal properties of the composites vary with QD loading (Figure 4). The pure NOA film decomposes to nearly zero mass after heating to 600 °C, indicating complete decomposition of the polymer upon thermal exposure (Figure 4a). Pure BAQD samples show weight loss up to 600 °C with >80% of the sample still remaining at this temperature. The initial weight loss is attributed to the organic fraction of the QDs (butylamine ligand has a boiling point of 78 °C),[50] although there is still weight loss taking place up to 450 °C; this can be attributed to tightly bound ligand leftover from the ligand exchange. The residual mass upon completion of the run at 600 °C is due to pure CdSe/$Cd_{1-x}Zn_xSe_{1-y}S_y$ QDs, around 78 wt %, as the boiling point for a bulk semiconductor of this nature is well beyond the experimental conditions. Similarly, the NOA-BAQD sample decomposition begins at 100 °C and follows a trajectory between that of the pure BAQDs and pure NOA samples. There is some variation in the thermal stability for the composite samples between 100 and 300 °C; weight loss in this region is typically due to organic content, suggesting minor variations in the amount of organic present. Depending on the concentration of QDs in the composite samples, TGA shows decomposition until all polymer is completely removed, leaving behind the pure thermally stable QD.

DSC shows no detectable T_g or T_m (within the temperature range of experiment) for the neat BA-QD sample, while the NOA polymer has a T_g of ca. 30 °C (Figure 4b).[51] The T_g of the QD−polymer composite depends on the fraction of QDs in the composite, with the T_g gradually decreasing as more QDs are introduced into the polymer composite. The decrease in T_g is counterintuitive given that the addition of hard semiconducting component to a polymer matrix typically results in an increase of T_g due to common reinforcing effect with inorganic reinforcing components.[2,52] In contrast, our results

DOI: 10.1021/acsami.7b03366
ACS Appl. Mater. Interfaces 2017, 9, 17435−17448

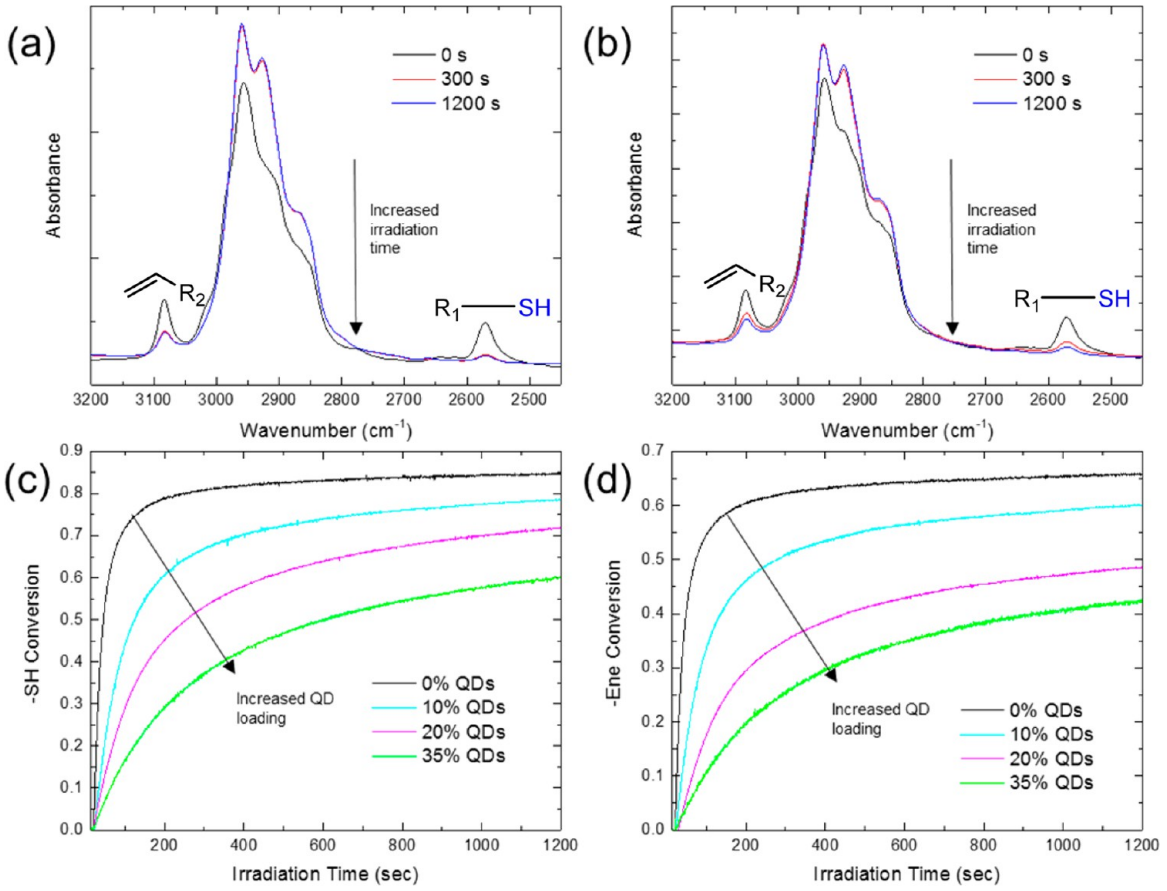

Figure 5. Representative time-lapsed FTIR showing reduction in $-C{=}CH_2$ (ene at ~3080 cm^{-1}) and −SH (thiol at ~2570 cm^{-1}) with more UV irradiation time for both (a) neat NOA and (b) NOA-BAQD composite. Conversion of both (c) −ene and (d) −thiol groups for neat NOA and NOA-BAQD with increasing concentrations of QDs clearly shows suppressed conversions.

suggest that the cross-linking density of the composite decreases with some type of plasticization effect taking place in the QD system as will be further discussed below.[40]

To understand the cross-link density of the nanocomposite system, real time infrared (RTIR) spectroscopy was used to observe the conversion of the vinyl (ene) and thiol (SH) functional groups as a function of irradiation time.[37,53−55] Typical RTIR spectra for the NOA and NOA-BAQD composite at various irradiation times can be seen in Figures 5a and 5b, respectively, emphasizing the ene peak at ~3100 cm^{-1} and the thiol peak at ~2570 cm^{-1}. The conversion as a function of irradiation time for both thiol and ene can also be seen in Figures 5c and 5d, respectively.

It can be clearly observed that the intensity of the thiol and ene peaks are reduced with increased irradiation time (Figures 5a and 5b). Taking the conversion as the change in area under these specific peaks, Figures 5c and 5d show a clear trend that the conversion and loading percentage are inversely proportional. Initially, with the neat NOA the conversion for the thiol and ene functional groups is nearly complete after 300 s. Notably, the conversion does not reach 100% (the thiol reaching ~85% and ene reaching ~66% after 1200 s), which is due to the dense cross-linked network achieved, as the gel point for typical formulations is ~40%, limiting mobility, and the conversion of both functional groups is not the same.[70] While previously observed systems typically show the ene being the dominant constituent as a significant amount of ene monomers can homopolymerize, for the current adhesive that is not the case.[54] The specific ally ether used, triallyl isocyanurate, does not possess the ability to homopolymerize;[56] however, high cross-linking densities are still achieved in the neat polymers. Upon addition of QDs significant reduction in conversion/cross-linking occurs, with conversion exceeding 50% for −SH upon addition of 35 wt % QDs.

It is worth noting that similar systems have been investigated, in which functionalized nanoparticles are incorporated into a polymer matrix, and the inclusion of nanoparticles does not typically disrupt the polymerization kinetics. However, if the nanoparticles are functionalized with a ligand that can participate in the photopolymerization reaction or there is a strong affinity between the nanoparticle surface and the functional group of the monomers being used, in this case a thiol or an ene, kinetics can be altered.[37,57] Specifically, Phillips et al. noted a strong interaction between the thiol−gold surface, limiting the availability of thiols in their particular system to react with ene monomers.[37] Herein, this is not the case, although it has been shown that thiols will have a strong affinity to the surface of QDs;[58] UV exposure of a tetrathiol, pentaerythritol tetrakis(3-mercaptopropionate), with photoinitiator irgacure 651, in the presence of BAQDs resulted in no appreciable change in the thiol peak using FTIR over a period of 15 min, suggesting the thiol does not tether to the QD surface.

However, the QD nanoparticles are significant light absorbers, given the typical quantum yield of these QDs around 30% and strong absorption in near-visible range (Figure

DOI: 10.1021/acsami.7b03366
ACS Appl. Mater. Interfaces 2017, 9, 17435−17448

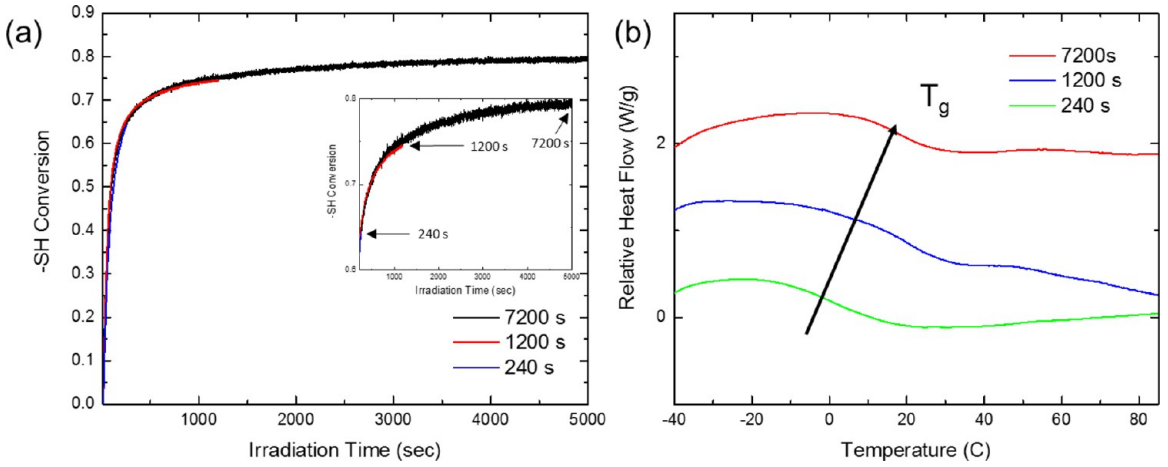

Figure 6. (a) Conversion of thiol groups for NOA-BAQD with 10 wt % QDs at different irradiation times showing the time dependence of the conversion of functional groups (inset shows a zoom-in of final conversion). (b) DSC plots showing the shift in T_g with increased irradiation time.

2).[40] Because the polymerization is initiated using 365 nm light, the QDs absorb a significant quantity of the irradiated light, thereby retarding the reaction. One important thing to note is a typical gelation point for similar multifunctional thiol−ene mixtures occurs around 40% conversion. Thereafter, the polymerization kinetics are severely hindered as a semisolid has formed; however, significant hampering of reaction kinetics take place well prior to this point upon incorporation of QD components.[56,59]

To further analyze these changes, we used the absorbance at 365 nm to calculate the fractional absorbance (Figure 2).[60] The QDs by themselves absorb about ∼39% of the light at this wavelength, while addition of an aliquot of NOA monomer solution, making the final solution similar to that of ∼10 wt % NOA-BAQD sample, resulted in a very negligible increase in the amount of light absorbed to ∼40%. Furthermore, absorbance measurements were done on solutions of varying concentrations in order to calculate the molar absorptivity at 365 nm. The calculated value, which was on the order of 10^6 mol^{-1} cm^{-1} for these particular CdSe-based QDs, similar to values previously obtained, suggest significant attenuation of the light as it travels through the composite film.[61] While it appears that the QDs absorb majority of the irradiated light that is used to initiate the polymerization of NOA, the reduction in conversion (cross-links) does not necessarily equate to a reduction in T_g.

A reduction in cross-linking density could result in a decreased T_g; however, several other factors can affect the T_g of cross-linked polymers.[62,63] In order to determine the effect of the conversion on the T_g, three 10 wt % NOA-BAQD samples were irradiated with UV light for varying times: 240, 1200, and 7200 s. Following each exposure, samples were analyzed with DSC to determine the T_g (Figure 6).

Figures 6a and 6b show the −SH conversion for samples irradiated and the DSC curve for each sample, respectively. While none of the samples reached the thiol conversion of the neat NOA (∼85%), the longer the samples were irradiated, the higher the conversion, with a maximum conversion of ∼80% reached for the sample irradiated for 7200 s. Correspondingly, Figure 6b shows an increase in T_g with longer irradiation times. Again the T_g does not recover to that of the neat NOA (30 °C for neat NOA vs 20 °C 10 wt % sample irradiated for 7200 s). Although near complete recovery of the T_g could be observed with longer irradiation times, it is not expected due to the mismatch in polarity between the monomer constituents and QD ligand.

Indeed, it has been established that a nonwetting interface between a hard surface and a polymer can result in a reduction of T_g as a result of confinement, network disruption, and formation of highly mobile polymer domains at the interface.[64−66] As mentioned, Ash et al. performed an in situ free-radical polymerization in which methyl methacrylate monomers were polymerized in the presence of alumina nanospheres capped with a silane capping agent, ranging in size from 17 to 38 nm, to form a PMMA−alumina nanocomposite. A decrease in T_g of nearly 25 °C was observed with as little as 0.5 wt % alumina incorporated into the composite system. The reduction in T_g was attributed solely to contributions from the nanoparticles, as removal of the alumina resulted in the T_g returning to that of the neat polymer. Dewetting at the interface between alumina and PMMA results in the nanoparticles creating nanoporosity throughout the composite, causing an overall disruption of the polymer network and an increased number of polymer islands with enhanced mobility near the QD−polymer interface.[48] Similarly, Bansal et al. observed a reduction in T_g for a polymer composite consisting of polystyrene and silica nanoparticles that was dependent on the interparticle spacing.[67] A consistent reduction of T_g was observed as the interparticle spacing was reduced, which was not observed when the surface of the filler was functionalized to better wet the polymer. In the case of the NOA-BAQD system, though the T_g can be partially recovered with extended irradiation times, there is a permanent decrease in T_g that gets larger as more QDs are added to the system. In accordance with previous studies, the addition of more QDs into the polymer appears to reduce the interparticle spacing, enhance polymer confinement, and create CRRs, resulting in localized nanoscale phase separation in which nanoscale regions of a highly mobile phase exists at the QD−polymer interface. One significant difference in the current system is that the monomer mixture is composed of all cross-linkers, which were initially thought to enhance dispersion.

Demir et al.[68] observed significant enhancement in nanoparticle dispersion in a PMMA matrix upon addition of a difunctional cross-linker. These changes were attributed to difunctional cross-linkers slowing down the diffusion of nanoparticles to form aggregates. While it was envisioned in this study that addition of multifunctional cross-linkers would

DOI: 10.1021/acsami.7b03366
ACS Appl. Mater. Interfaces 2017, 9, 17435−17448

create a diffusion limited system which would severely limit QD aggregation, there appears to be some incompatibility at the interface between QD and monomers which leads too nanoscale aggregation. It is worth noting that the filler particles can be treated for better wetting with the polymer.

While the current monomer/ligand selection does appear to demonstrate a nonwetting interface, and a T_g that is not completely recoverable, the thermal properties can still be controlled to an extent. The variability of T_g indicates that the polymer composite can be changed from a rigid state to a more soft and flexible state as a function of the irradiation time, while still remaining as a robust, intact polymer composite. To demonstrate the flexible nature of the QD composite, films were detached from silicon substrates and suspended in fluid and bent with tweezers (Figure S5). Understanding the thermal properties of composite systems enables tailoring of the composite structure for a given application (i.e., waveguides and lasers), which is particularly important when designing optical systems on flexible substrates.

Kinetics of Polymerization. Further analysis of the RTIR data allowed for more in-depth understanding of the polymerization. The rate of propagation, also termed the rate of polymerization, R_p, can be calculated as follows: $R_p = d[M]/dt$, where [M] is the monomer concentration. R_p is typically calculated from the ene conversion curve, using the initial slope of the conversion data in Figure 5d (Table 1).[37]

Table 1. Effect of QD Concentration on Rate of Polymerization and Final Conversion of Ene

sample (wt %)	rate of polymerization (s^{-1})	final conversion (%)
0	0.015	66
10	0.006	60
20	0.003	48
35	0.001	42

As was shown previously, and further corroborated here with kinetics analysis, significant retardation of the polymerization rate occurs upon addition of QDs to the system. Assuming a standard photoinitiated polymerization, the rate of polymerization and the rate of initiation, R_i, are proportional, i.e., $R_p \propto R_i^{0.5}$, with R_i being influenced by a number of things including concentration, efficiency, and light intensity.[69] Light is strongly attenuated as the concentration of QDs is increased, limiting the amount of light available to initiate the polymerization and form free radicals. Furthermore, using the conversion the reaction order of this composite system was determined.

Assuming an overall first-order reaction, being half-order in terms of each monomer, $\log(1 - x)$, where x is the ene conversion, was plotted as a function of time (Figure 7). While the majority of the thiol−ene formulations tend to follow a first-order reaction rate, that does not appear to be the case here. As was previously shown, addition of QDs to the monomer formulation results in a significant decrease in the amount of UV light available for the photoinitiatior to absorb, given that the QDs are the dominating component. As a result, the polymerization proceeds via a two stages with different rates: the polymerization initially proceeds at one rate, and upon reaching the gelation point this rate is severely hindered. As mentioned, the critical gel point for thiol−ene chemistries of this functionality is ∼40%; for the neat polymer this is reached within 40 s.[70]

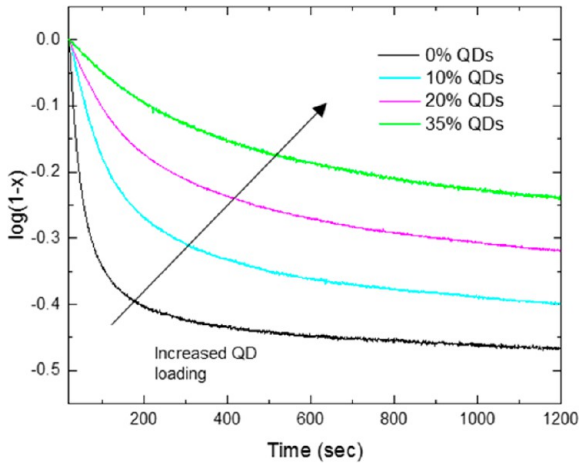

Figure 7. Plot of $\log(1 - x)$ as a function of UV irradiation time showing initial first-order reaction kinetics.

In our case, fitting analysis reveals that the polymerization kinetic transition from one exponential decay to another well beyond 40 s. For the neat polymer, it appears that an additive of the adhesive could be perturbing the reaction, resulting in a nonlinear polymerization rate. As QDs are added to the prepolymer mixture, less light is available to be absorbed by the photoinitiator; thereby less free radicals are generated, resulting in a much slower reaction than what is to be expected from your traditional free-radical, step-growth-like polymerization.

Mechanical Properties of QD−Polymer Films. Force spectroscopy measurements were conducted via an AFM nanomechanical probing to further corroborate the observed change in the thermal and mechanical properties. In this case, force−distance curves were gathered from thin films suspended across a circular aperture in order to calculate tensile elastic modulus in accordance with the well-known approach (Figure 8).[71−74]

Based on the load−deflection characteristics of the polymer thin films, the elastic modulus of the neat polymer NOA film was found to be 16.4 ± 2.5 GPa, with no significant changes in the modulus value observed upon addition of 0.5 wt % BA-QDs (Figure 8d). It is worth noting that initial values are higher than that expected for the neat polymer film and can be related to large initial deformation during tip jump-in initial contact.[35] However, above 0.5 wt % QDs there is a drastic threshold like decrease of the modulus down to 5.0 ± 0.52 GPa. At the highest loading measured (33 wt %), the modulus the highest loading measured (33 wt %); the modulus drops even further, to 1.2 ± 0.44 GPa (Figure 8d).

Drop in the elastic modulus for polymer composites has been observed in several studies after adding inorganic components. For instance, Bowman et al. showed a clear correlation between glass transition temperature and resulting modulus, depending on the thiol−ene/thiol−acrylate monomer constituents used, with lower T_g's resulting in lower moduli.[33] Herein, the lower the conversion/cross-linking, the lower the T_g, and corresponding moduli. Furthermore, it has been shown that increased cross-linking results in enhanced mechanical properties and vice versa.[75] The continued reduction of elastic modulus with increased loading suggests that the cross-linking density of the polymer matrix is being altered, causing a change in mechanical properties.[33] As was confirmed by FTIR and UV−vis, an increase in QD loading results in a significant portion of the UV

DOI: 10.1021/acsami.7b03366
ACS Appl. Mater. Interfaces 2017, 9, 17435−17448

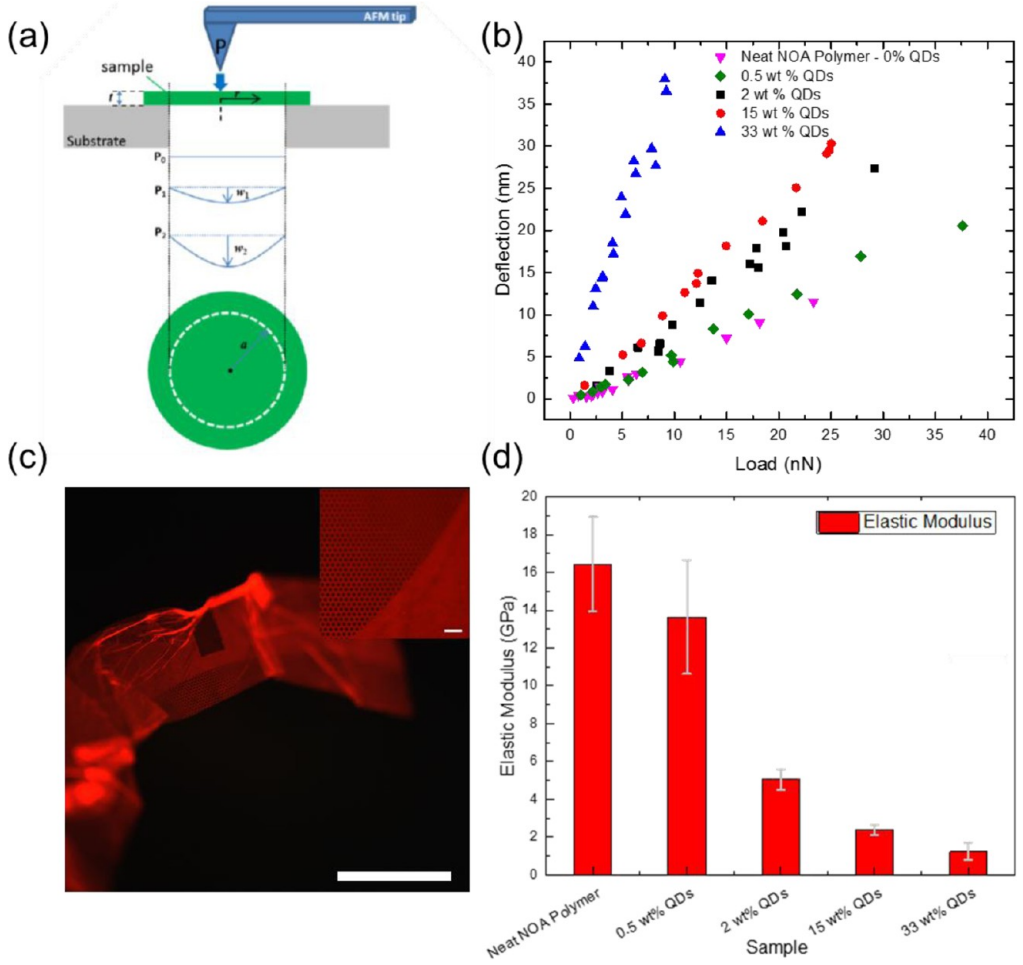

Figure 8. Force spectroscopy experimental setup (a) in which a point load is applied to a thin film suspended across a circular aperture using an AFM probe. (b) Representative Force-Distant curves showing difference between QD loaded polymers. (c) Wrinkled NOA-BAQD film suspended across the edge of a TEM grid, inset is zoomed in image of composite film on grid. (d) Elastic modulus for films with varying QD loading, measured using force spectroscopy. Scale bars: 50 μm.

Scheme 2. Soft Lithographic Techniques Exploited in This Study: (a) MIMIC and (b) μTM, in Which a Very Dilute Monomer Solution is Used To Create Patterns on the Submicrometer Scale

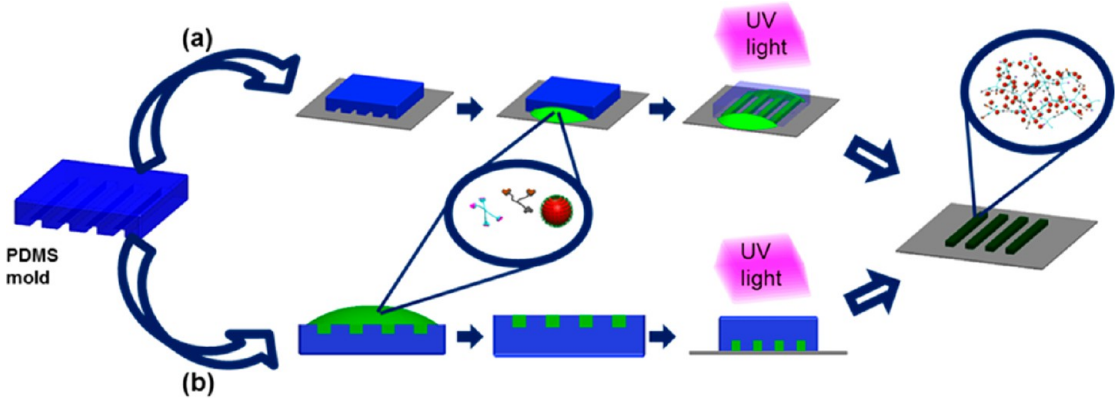

light, used to initiate the polymerization, being absorbed by the QDs. Although it has also been shown that a reduction of the Young's modulus in nanocomposites has resulted due in part to the same reason a reduction in T_g is observed, weak interface and, in some cases, cavitation at the interface,[28] in this study it appears that the cross-linking plays a significantly larger role.

These results clearly show that the physical properties of the QD−polymer composite vary drastically with QD loading fraction and UV irradiation time. Both glass transition and mechanical strength decrease significantly as a result of adding quantum dots and decreasing cross-linking density and polymerization progression. This approach, thus, can be used to reliably control the mechanical properties of these composite

DOI: 10.1021/acsami.7b03366
ACS Appl. Mater. Interfaces 2017, 9, 17435−17448

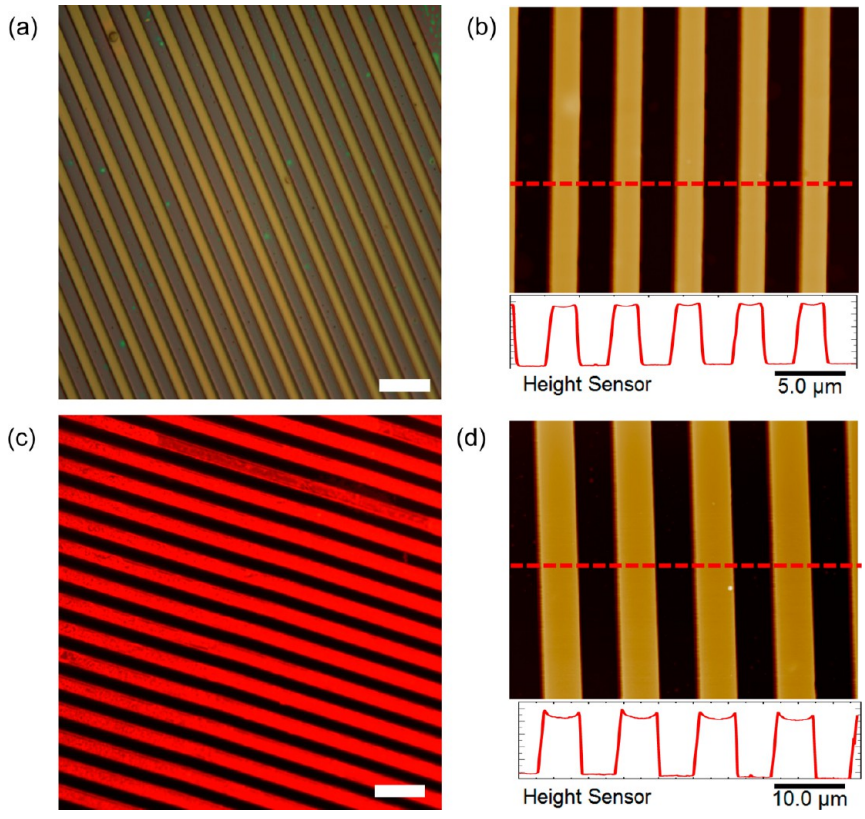

Figure 9. Bright-field (a) and AFM topography (b) images of soft lithographic patterns of neat NOA63 polymer. Fluorescence (c) and AFM topography (d) images of soft lithographic patterns of neat BAQD-NOA63 polymer composite. Optical image scale bars: 20 μm; AFM maximum height: 1 μm.

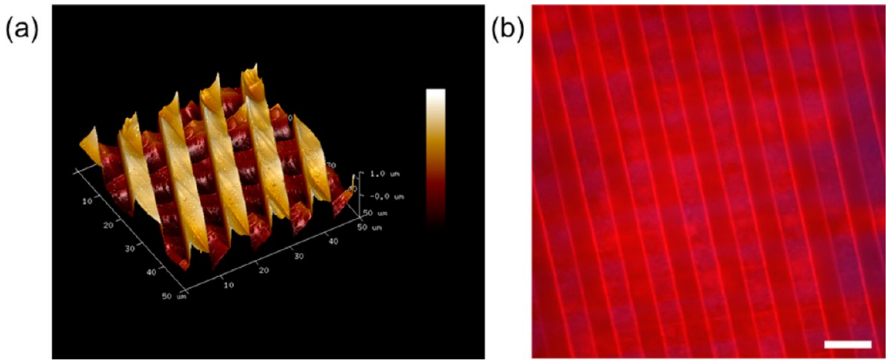

Figure 10. AFM scan (a) showing 3D structure prepared using complimentary soft lithography techniques and (b) Fluorescence imaging showing a layered structure consisting of red emitting and blue emitting waveguide strips. Scale bar: 20 μm.

films without requiring the inclusion of additional chemical additives (reinforcing or plasticizing) that could alter the optical properties, typically caused by large-scale phase separation in QD−polymer systems.

QD−Polymer Film Patterning with Soft Lithography. To demonstrate the feasibility and compatibility of the NOA-BAQD mixture for making robust and low optical loss waveguide and cavity like structures and patterns, we exploited soft lithographical approaches. Two patterning methods were utilized here: micromolding in capillary (MIMIC) and microtransfer molding (μTM) (Scheme 2).[76]

The benefits of these techniques include the ability to fabricate high aspect ratio, sharp featured free-standing patterns that can be sequentially repeated to produce complex physical patterns. These two techniques are complementary to each other since they both can be used to generate three-dimensional structures.[76] Given the fluid-like nature of the initial monomer−QD mixture, capillary forces can readily pull the mixture into the columnar structures of polydimethylsiloxane (PDMS) stamps during traditional microprinting.[76−78] In the first fabrication approach, a PDMS stamp is placed on a substrate (typically a silicon wafer). A drop of a 1 wt % polymer solution with QDs is placed next to the columnar openings of the PDMS stamp, and capillary forces pull the solution into the stamp (Scheme 2a). Prior to irradiating with UV light, the solution inside the stamp is degassed. Following UV irradiation, the stamp is simply peeled off, leaving behind a QD−polymer composite pattern on the substrate.

In another approach, the monomer−QD solution is instead placed directly on top of the PDMS stamp, followed by

DOI: 10.1021/acsami.7b03366
ACS Appl. Mater. Interfaces 2017, 9, 17435−17448

capillary forces pulling solution into the recessed regions, and removal of any excess solution (Scheme 2b). The polymerization then proceeds as in the previous approach used to produce a thin film. Patterns of neat polymer and polymer−QD composites can be seen in bright-field and fluorescence optical images and AFM scans in Figure 9.

QD−polymer patterns generated here display very sharp submicrometer to micrometer scale patterns with controlled and consistent physical characteristics (width, height, and spacing) over large surface areas of mm^2. A variety of single-layer and multilayers patterns can be fabricated, including strips/waveguides and holes. Multilayer patterns fabricated using both methods in Scheme 2 can be seen in Figure 10, AFM and fluorescence imaging confirm layered structure and emissive nature.

3. CONCLUSIONS

This work has demonstrated a facile technique using thiol−ene chemistry to incorporate QDs into a polymer matrix in controllable and uniform manner with suppressed large-scale aggregation of QDs. Taking advantage of shorter QD ligands with simple alkane backbones makes it feasible to embed QDs within a polymer matrix without noticeable phase separation. The incorporation of QDs into polymer matrixes results in reduced and controllable light absorption, and thus, controllable cross-linking that allows one to adjust the mechanical and thermal properties, making QD−polymer composite with unusually high QD load (>30% instead of common composites, <1%). Composites are rather flexible and behave as elastomeric-like materials with high optical clarity, low optical losses, and high, uniform photoluminescent emission.

Moreover, we demonstrated that traditional microprinting methods can be applied to the materials in order to fabricate complex 3D highly emissive patterns. Overall, this approach yields highly emissive and optically stable films with minimal optical scattering due to the nanoscale phase separation, which maintaining the optical capabilities of the QDs. The significant reduction in modulus allows for the composite to be formed on nonplanar or flexible substrates or on its own as a robust free-standing and flexible film. These commercial optical adhesives are extremely low cost and robust and offer the ability to tune mechanical and thermal properties via selection of initial monomer chemistry and control of exposure parameters.

4. EXPERIMENTAL METHODS

Chemicals and Materials. Cadmium oxide, tri-*n*-octylphosphine (TOP, 90%), and selenium powder were obtained from Sigma-Aldrich. 1-Tetradecylphosphonic acid (TDPA, 98%), tri-*n*-octylphosphine oxide (TOPO, 90%), diethylzinc (15 wt % in hexane), hexane, and chloroform were obtained from Alfa Aesar. 1-Octadecene (ODE, 90%), hexadecylamine (HDA, 90%), butylamine (BA, 98%), oleic acid (OA, 97%), and bis(trimethylsilyl) sulfide (95%) were obtained from TCI. Norland Optical Adhesive 63 was obtained from Edmund Optics. All chemicals were used as received.

Synthesis of Compositional Gradient CdSe/$Cd_{1-x}Zn_xSe_{1-y}S_y$ QDs. Chemical composition gradient CdSe/$Cd_{1-x}Zn_xSe_{1-y}S_y$core/alloyed-shell QDs were synthesized by a previously reported method.[3] Briefly, 0.2 mmol of CdO, 4 mmol of Zn(acetate)2, 5 mL of oleic acid, and 15 mL of 1-octadecene (ODE) were placed in a three-necked flask and degassed at 150 °C for 1 h. The reaction was heated to 300 °C under Ar. At the elevated temperature (300 °C), 1 mmol of Se and 4 mmol of S in 2 mL of TOP were rapidly injected into the reaction vessel. The reaction was allowed to proceed at 300 °C for 10 min, and then the heating mantle was removed to stop the reaction. 5 mL of hexane was added to the solution once the temperature reached 70 °C.

Ligand Exchange. The oleic acid-capped CdSe/$Cd_{1-x}Zn_xSe_{1-y}S_y$ QDs were centrifuged with acetone three times to remove excess oleic acid and ODE. Subsequently, purified oleic acid-capped CdSe/$Cd_{1-x}Zn_xSe_{1-y}S_y$ QDs were redispersed in chloroform, and an excess amount of butylamine was added to perform the solution-phase ligand exchange. The ligand exchange reaction was allowed to proceed at 45 °C for 1 day. The solution was then precipitated using methanol and redispersed in a mixture of chloroform and an excess amount of BA. This procedure was repeated three times.[79]

Film Preparation. QD films were fabricated by first mixing a QD chloroform solution of a known quantity with an equal volume 10 wt % NOA solution in chloroform and spin-casting at 3000 rpm for 1 min. The film thickness ranged from 250 to 400. Silicon, with a 290−295 nm thick SiO_2 surface layer, was used as a substrate. Films were polymerized using Omnicure X-Cite Series 120Q mercury vapor arc lamp.

Real Time Fourier Transform Infrared Spectroscopy. FTIR measurements of NOA and NOA-BAQD composites were conducted using a Nicolet iS50 FTIR in accordance with a procedure previously described.[53] A known quantity of sample was deposited on a NaCl crystal and dried prior to each run for transmission mode. FTIR spectra were collected in the range of 3200−2450 cm^{-1} with a resolution 8 cm^{-1}. Series spectra were collected every half second. Polymerizations were initiated using a LED lamp (OmniCure LX 500) with a 365 nm wavelength. Samples were irradiated until polymerization was complete, indicated by very negligible change in peaks observed. During each reaction the absorbance peaks corresponding to the vinyl group (3080 cm^{-1}) and thiol group (2570 cm^{-1}) were observed as a function of time. The typical allyl peak (1646 cm^{-1}) was not monitored because the intensity was too low. The conversion ratio was taken as the peak area at time t to the peak area before polymerization began. Experiments were conducted in ambient conditions.

Optical Characterization. UV−vis extinction spectra of QD solutions (quartz cuvette) from 350 to 900 nm (1 nm intervals) were collected using a Shimadzu UV-vis-2450 spectrometer with D2 and tungsten lamps offering a wavelength range of 300−1100 nm. The QD extinction spectra were corrected against the pure solvent background and the same quartz cuvette. Photoluminescence spectra of QD solutions and composite films were collected using a Shimadzu fluorescent RF-5301PC spectrofluorophotometer with the excitation wavelength of 525 nm. Photoluminescence (PL) images were collected using a Dagexcel-M Digital Firewire camera (cooled). All PL imaging was performed using photoluminescence excitation from a blue bandpass filter (450−490 nm) with a dichroic mirror that reflects optical wavelengths below 495 nm and with a long-pass emission filter that passes optical wavelengths above 500 nm. The light source is a mercury vapor arc lamp providing a wavelength range of 250−800 nm and a power of 120 W of nonpolarized light.

Fabrication of QD Patterns. Briefly, a known quantity of QDs in solution was added to a 2 wt % NOA solution in chloroform. Typically, a 1 cm^2 cutout of a PDMS stamp was placed on a silicon substrate, and a small aliquot of the NOA-BAQD solution was injected next to the stamp to allow capillary forces to pull solution in or the solution was injected on top of the stamp followed by placing of the stamp on the substrate, in accordance with a procedure previously described. Samples were polymerized using an Omnicure X-Cite Series 120Q mercury vapor arc lamp.

Atomic Force Microscopy. AFM images were collected using a Dimension Icon microscope (Bruker) in tapping mode according to a procedure previously described.[80] MikroMasch pyramidal silicon tips were used with a height of 15 μm, a cantilever length of 150 μm, and a spring constant of 7 N/m. Scan size ranged from 50 μm by 50 μm to 500 nm by 500 nm with a scan rate within 0.3−0.8 Hz.[42]

Differential Scanning Calorimetry. The heat flow as a function of temperature of the DIAH-tethered QD sample was measured using a TA Instruments DSC Q200 with hermitically sealed aluminum pans. Samples were analyzed from −50 to 200 °C using a 10 °C/min temperature profile under a constant flow of argon.

DOI: 10.1021/acsami.7b03366
ACS Appl. Mater. Interfaces 2017, 9, 17435−17448

Thermogravimetric Analysis. The sample weight as a function of temperature of the composite QD samples was measured using a TA Instruments TGA Q50 with a 100 μL platinum pan. Samples were analyzed from RT to 600 °C using a 10 °C/min temperature profile under a constant flow of argon.

Transmission Electron Microscopy. The CdSe/$Cd_{1-x}Zn_xSe_{1-y}S_y$ QDs were studied using a high-resolution transmission electron microscope (Tecnai F30). An accelerating voltage of 300 keV was used. TEM samples were prepared by diluting the original QD solution of ~6 mg/mL 30 times. Then, 5−10 μL of the diluted solution was drop-cast on the TEM grid and allowed to dry completely.

Force−Distance Measurements. Force−distance measurements were performed to analyze the mechanical properties of NOA-BAQD composites, which were freely suspended on the copper-TEM grids with circular aperture size of 10 μm. The deflection sensitivity of the AFM tip was obtained by conducting force−distance experiment on a sapphire substrate. The spring constant of the AFM tip was determined by using the thermal tune method.[81] The radius of the AFM tip was obtained by deconvoluting the images on 20 nm gold nanoparticles.[42] The force−distance curves were obtained with various ramp rates of 0.2, 0.4, 0.6, 0.8, 1.0, 2.0, 4.0, 6.5, and 10 Hz.

Quantum Yield Measurement. Quantum yields of QDs dispersed in chloroform are determined by the relative quantum yield method reported in the literature.[82] A standard sample, rhodamine 101 (QY = 91.5%), dissolved in ethanol was used to determine QDs emitting at red regions. UV−vis extinction spectra of QD solutions (quartz cuvette) from 350 to 900 nm (1 nm intervals) were collected using a Shimadzu UV-vis-2600 spectrometer with D2 and tungsten lamps offering a wavelength range of 300−1100 nm. The QD extinction spectra were corrected against the pure solvent background and the same quartz cuvette. Photoluminescence spectra of QD solutions were collected using a Shimadzu fluorescent RF-5301PC spectrofluorophotometer with the excitation wavelengths of 525 nm. All of the extinction values of solutions are diluted to be less than 0.1 before measurement in order to avoid the reabsorption effect.

Scanning Electron Microscopy. SEM characterization was performed on a Hitachi S-3400N SEM with a backscattering electron detector with an accelerating voltage in the range 10−15 kV. Films were sputtered with gold prior to being imaged.

X-ray Diffraction. XRD measurements were performed on a X'Pert PRO Alpha-1 diffractometer (PANalytical) using the Cu Kα_1 component.

■ ASSOCIATED CONTENT

Supporting Information

The Supporting Information is available free of charge on the ACS Publications website at DOI: 10.1021/acsami.7b03366.

(PDF)

■ AUTHOR INFORMATION

Corresponding Author

*E-mail: Vladimir@mse.gatech.edu (V.V.T.).

ORCID

Timothy J. White: 0000-0001-8006-7173

Zhiqun Lin: 0000-0003-3158-9340

Vladimir V. Tsukruk: 0000-0001-5489-0967

Notes

The authors declare no competing financial interest.

■ ACKNOWLEDGMENTS

Financial support is acknowledged from the Air Force Office of Scientific Research FA9550-14-1-0037 (Synthetic photonics Multidisciplinary University Research Initiative: synthesis, fabrication, and development) and the U.S. Department of Energy, Office of Basic Energy Sciences, Division of Materials Sciences and Engineering Award # DE-FG02-09ER46604 (optical measurements and QD characterization). M. J. Smith acknowledges the Science, Mathematics, and Research for Transformation (SMART) scholarship funded by Office of Secretary Defense-Test and Evaluation (OSD-T&E), Defense-Wide/PE0601120D8Z National Defense Education Program (NDEP)/BA-1, Basic Research, SMART Program office grant N00244-09-1-0081. We thank Professor Dong Qin (Georgia Institute of Technology) for assisting in the fabrication of the patterned PDMS molds and providing the master Cr-on-quartz master pattern.

■ REFERENCES

(1) Talapin, D. V.; Lee, J.-S.; Kovalenko, M. V.; Shevchenko, E. V. Prospects of Colloidal Nanocrystals for Electronic and Optoelectronic Applications. *Chem. Rev.* **2010**, *110*, 389−458.

(2) Sperling, L. H. *Introduction to Physical Polymer Science*; John Wiley & Sons: 2005.

(3) Jung, J.; Lin, C. H.; Yoon, Y. J.; Malak, S. T.; Zhai, Y.; Thomas, E. L.; Vardeny, V.; Tsukruk, V. V.; Lin, Z. Crafting Core/Graded Shell−Shell Quantum Dots with Suppressed Re-absorption and Tunable Stokes Shift as High Optical Gain Materials. *Angew. Chem., Int. Ed.* **2016**, *55*, 5071−5075.

(4) Li, Q.; Zhou, H.; Hoyle, C. E. The Effect of Thiol and Ene Structures on Thiol-Ene Networks: Photopolymerization, Physical, Mechanical and Optical Properties. *Polymer* **2009**, *50*, 2237−2245.

(5) Greytak, A. B.; Allen, P. M.; Liu, W.; Zhao, J.; Young, E. R.; Popovic, Z.; Walker, B. J.; Nocera, D. G.; Bawendi, M. G. Alternating Layer Addition Approach to CdSe/CdS Core/Shell Quantum Dots with Near-Unity Quantum Yield and High On-Time Fractions. *Chem. Sci.* **2012**, *3*, 2028−2034.

(6) Sonawane, K. G.; Agarwal, K. S.; Phadnis, C.; Sharma, D.; Layek, A.; Chowdhury, A.; Mahamuni, S. Manifestations of Varying Grading Level in CdSe/ZnSe Core-Shell Nanocrystals. *J. Phys. Chem. C* **2016**, *120*, 5257−5264.

(7) Bae, W. K.; Park, Y.-S.; Lim, J.; Lee, D.; Padilha, L. A.; McDaniel, H.; Robel, I.; Lee, C.; Pietryga, J. M.; Klimov, V. I. Controlling the Influence of Auger Recombination on the Performance of Quantum-Dot Light-Emitting Diodes. *Nat. Commun.* **2013**, *4*, 2661−2998.

(8) Chuang, C.-H. M.; Brown, P. R.; Bulovic, V.; Bawendi, M. G. Improved Performance and Stability in Quantum Dot Solar Cells through Band Alignment Engineering. *Nat. Mater.* **2014**, *13*, 796−801.

(9) Meinardi, F.; McDaniel, H.; Carulli, F.; Colombo, A.; Velizhanin, K. A.; Makarov, N. S.; Simonutti, R.; Klimov, V. I.; Brovelli, S. Highly Efficient Large-Area Colourless Luminescent Solar Concentrators Using Heavy-Metal Free Colloidal Quantum Dots. *Nat. Nanotechnol.* **2015**, *10*, 878−885.

(10) Lin, C. H.; Lafalce, E.; Jung, J.; Smith, M. J.; Malak, S. T.; Aryal, S.; Yoon, Y. J.; Zhai, Y.; Lin, Z.; Vardeny, Z. V.; Tsukruk, V. V. Core/Alloyed-Shell Quantum Dot Robust Solid Films with High Optical Gains. *ACS Photonics* **2016**, *3*, 647−658.

(11) Mashford, B. S.; Stevenson, M.; Popovic, Z.; Hamilton, C.; Zhou, Z. Q.; Breen, C.; Steckel, J.; Bulovic, V.; Bawendi, M.; Coe-Sullivan, S.; Kazlas, P. T. High-Efficiency Quantum-Dot Light-Emitting Devices with Enhanced Charge Injection. *Nat. Photonics* **2013**, *7*, 407−412.

(12) Malak, S. T.; Jung, J.; Yoon, Y. J.; Smith, M. J.; Lin, C. H.; Lin, Z.; Tsukruk, V. V. Large-Area Multicolor Emissive Patterns of Quantum Dot−Polymer Films via Targeted Recovery of Emission Signature. *Adv. Opt. Mater.* **2016**, *4*, 608−619.

(13) Maragkou, M. Colloidal Quantum Dots: Long-Lived Lasing. *Nat. Mater.* **2015**, *14*, 1186−1186.

(14) Wood, V.; Panzer, M. J.; Chen, J. L.; Bradley, M. S.; Halpert, J. E.; Bawendi, M. C.; Bulovic, V. Inkjet-Printed Quantum Dot-Polymer Composites for Full-Color AC-Driven Displays. *Adv. Mater.* **2009**, *21*, 2151−2155.

(15) Reithmaier, J. P.; Sek, G.; Loffler, A.; Hofmann, C.; Kuhn, S.; Reitzenstein, S.; Keldysh, L. V.; Kulakovskii, V. D.; Reinecke, T. L.;

Forchel, A. Strong Coupling in a Single Quantum Dot-Semiconductor Microcavity System. *Nature* **2004**, *432*, 197−200.
(16) Ramezani, H.; Kottos, T.; El-Ganainy, R.; Christodoulides, D. N. Unidirectional Nonlinear PT-Symmetric Optical Structures. *Phys. Rev. A: At., Mol., Opt. Phys.* **2010**, *82*, 043803-1−043803-6.
(17) Lin, Z.; Ramezani, H.; Eichelkraut, T.; Kottos, T.; Cao, H.; Christodoulides, D. N. Unidirectional Invisibility Induced by PT-Symmetric Periodic Structures. *Phys. Rev. Lett.* **2011**, *106*, 213901-1−213901-4.
(18) Song, J.; Li, J.; Xu, J.; Zeng, H. Superstable Transparent Conductive Cu@Cu4Ni Nanowire Elastomer Composites against Oxidation, Bending, Stretching, and Twisting for Flexible and Stretchable Optoelectronics. *Nano Lett.* **2014**, *14*, 6298−6305.
(19) Liu, Z.; Sun, Y.; Yuan, J.; Wei, H.; Huang, X.; Han, L.; Wang, W.; Wang, H.; Ma, W. High-Efficiency Hybrid Solar Cells Based on Polymer/PbSxSe1-x Nanocrystals Benefiting from Vertical Phase Segregation. *Adv. Mater.* **2013**, *25*, 5772−5778.
(20) Coe-Sullivan, S.; Steckel, J. S.; Woo, W. K.; Bawendi, M. G.; Bulovic, V. Large-Area Ordered Quantum-Dot Monolayers via Phase Separation during Spin-Casting. *Adv. Funct. Mater.* **2005**, *15*, 1117−1124.
(21) Wang, Y.; Ta, V. D.; Leck, K. S.; Tan, B. H. I.; Wang, Z.; He, T.; Ohl, C.-D.; Demir, H. V.; Sun, H. Robust Whispering-Gallery-Mode Microbubble Lasers from Colloidal Quantum Dots. *Nano Lett.* **2017**, *17*, 2640−2646.
(22) Kim, C.-H.; Bang, J.-H.; Hong, K. B.; Park, M.-H. Fabrication of Highly Photoluminescent Quantum Dot-Polymer Composite Micropatterned Surface Using Thiol-ene Chemistry. *RSC Adv.* **2016**, *6*, 96700−96705.
(23) Resch-Genger, U.; Grabolle, M.; Cavaliere-Jaricot, S.; Nitschke, R.; Nann, T. Quantum Dots Versus Organic Dyes as Fluorescent Labels. *Nat. Methods* **2008**, *5*, 763−775.
(24) Noh, M.; Kim, T.; Lee, H.; Kim, C.-K.; Joo, S.-W.; Lee, K. Fluorescence Quenching caused by Aggregation of Water-Soluble CdSe Quantum Dots. *Colloids Surf., A* **2010**, *359*, 39−44.
(25) Wang, Y.; Li, X.; Sreejith, S.; Cao, F.; Wang, Z.; Stuparu, M. C.; Zeng, H.; Sun, H. Photon Driven Transformation of Cesium Lead Halide Perovskites from Few-Monolayer Nanoplatelets to Bulk Phase. *Adv. Mater.* **2016**, *28*, 10637−10643.
(26) Ehlert, S.; Stegelmeier, C.; Pirner, D.; Förster, S. A General Route to Optically Transparent Highly Filled Polymer Nanocomposites. *Macromolecules* **2015**, *48*, 5323−5327.
(27) Vaidya, S. V.; Couzis, A.; Maldarelli, C. Reduction in Aggregation and Energy Transfer of Quantum Dots Incorporated in Polystyrene Beads by Kinetic Entrapment due to Cross-Linking during Polymerization. *Langmuir* **2015**, *31*, 3167−3179.
(28) Raja, S. N.; Luong, A. J.; Zhang, W.; Lin, L.; Ritchie, R. O.; Alivisatos, A. P. Cavitation-Induced Stiffness Reductions in Quantum Dot−Polymer Nanocomposites. *Chem. Mater.* **2016**, *28*, 2540−2549.
(29) Kade, M. J.; Burke, D. J.; Hawker, C. J. The Power of Thiol-Ene Chemistry. *J. Polym. Sci., Part A: Polym. Chem.* **2010**, *48*, 743−750.
(30) Lowe, A. B. Thiol-ene "Click" Reactions and Recent Applications in Polymer and Materials Synthesis. *Polym. Chem.* **2010**, *1*, 17−36.
(31) Chan, J. W.; Hoyle, C. E.; Lowe, A. B. Sequential Phosphine-Catalyzed, Nucleophilic Thiol−Ene/Radical-Mediated Thiol−Yne Reactions and the Facile Orthogonal Synthesis of Polyfunctional Materials. *J. Am. Chem. Soc.* **2009**, *131*, 5751−5753.
(32) Hoyle, C. E.; Bowman, C. N. Thiol-Ene Click Chemistry. *Angew. Chem., Int. Ed.* **2010**, *49*, 1540−1573.
(33) Carioscia, J. A.; Schneidewind, L.; O'Brien, C.; Ely, R.; Feeser, C.; Cramer, N.; Bowman, C. N. Thiol-Norbornene Materials: Approaches to Develop High T-g Thiol-Ene Polymers. *J. Polym. Sci., Part A: Polym. Chem.* **2007**, *45*, 5686−5696.
(34) Senyurt, A. F.; Wei, H.; Hoyle, C. E.; Piland, S. G.; Gould, T. E. Ternary Thiol-Ene/Acrylate Photopolymers: Effect of Acrylate Structure on Mechanical Properties. *Macromolecules* **2007**, *40*, 4901−4909.
(35) https://www.norlandprod.com/adhesiveindex2.html.
(36) Khire, V. S.; Benoit, D. S. W.; Anseth, K. S.; Bowman, C. N. Ultrathin Gradient Films using Thiol-Ene Polymerizations. *J. Polym. Sci., Part A: Polym. Chem.* **2006**, *44*, 7027−7039.
(37) Phillips, J. P.; Mackey, N. M.; Confait, B. S.; Heaps, D. T.; Deng, X.; Todd, M. L.; Stevenson, S.; Zhou, H.; Hoyle, C. E. Dispersion of Gold Nanoparticles in UV-Cured, Thiol-Ene Films by Precomplexation of Gold-Thiol. *Chem. Mater.* **2008**, *20*, 5240−5245.
(38) van Berkel, K. Y.; Hawker, C. J. Tailored Composite Polymer-Metal Nanoparticles by Miniemulsion Polymerization and Thiol-Ene Functionalization. *J. Polym. Sci., Part A: Polym. Chem.* **2010**, *48*, 1594−1606.
(39) Lü, C.; Cui, Z.; Wang, Y.; Li, Z.; Guan, C.; Yang, B.; Shen, J. Preparation and Characterization of ZnS/Polymer Nanocomposite Films with High Refractive Index. *J. Mater. Chem.* **2003**, *13*, 2189−2195.
(40) Malak, S. T.; Lafalce, E.; Jung, J.; Lin, C. H.; Smith, M. J.; Yoon, Y. J.; Lin, Z.; Vardeny, Z. V.; Tsukruk, V. V. Enhancement of Optical Gain Characteristics of Quantum Dot Films by Optimization of Organic Ligands. *J. Mater. Chem. C* **2016**, *4*, 10069−10081.
(41) Kagan, C. R.; Murray, C. B.; Bawendi, M. G. Long-Range Resonance Transfer of Electronic Excitations in Close-Packed CdSe Quantum-Dot Solids. *Phys. Rev. B: Condens. Matter Mater. Phys.* **1996**, *54*, 8633−8643.
(42) McConney, M. E.; Singamaneni, S.; Tsukruk, V. V. Probing Soft Matter with the Atomic Force Microscopies: Imaging and Force Spectroscopy. *Polym. Rev.* **2010**, *50*, 235−286.
(43) Sanchez, M. S.; Mateo, J. M.; Colomer, F. J. R.; Ribelles, J. L. G. Nanoindentation and Tapping Mode AFM Study of Phase Separation in Poly(ethyl acrylate-co-hydroxyethyl methacrylate) Copolymer Networks. *Eur. Polym. J.* **2006**, *42*, 1378−1383.
(44) Raghavan, D.; Gu, X.; Nguyen, T.; VanLandingham, M.; Karim, A. Mapping Polymer Heterogeneity using Atomic Force Microscopy Phase Imaging and Nanoscale Indentation. *Macromolecules* **2000**, *33*, 2573−2583.
(45) Magonov, S. N.; Elings, V.; Whangbo, M. H. Phase Imaging and Stiffness in Tapping-Mode Atomic Force Microscopy. *Surf. Sci.* **1997**, *375*, L385−L391.
(46) Luzinov, I.; Julthongpiput, D.; Malz, H.; Pionteck, J.; Tsukruk, V. V. Polystyrene Layers Grafted To Epoxy-Modified Silicon Surfaces. *Macromolecules* **2000**, *33*, 1043−1048.
(47) Luzinov, I.; Julthongpiput, D.; Tsukruk, V. V. Thermoplastic Elastomer Monolayers Grafted to a Silicon Substrate. *Macromolecules* **2000**, *33*, 7629−7638.
(48) Ash, B. J.; Siegel, R. W.; Schadler, L. S. Glass-Transition Temperature Behavior of Alumina/PMMA Nanocomposites. *J. Polym. Sci., Part B: Polym. Phys.* **2004**, *42*, 4371−4383.
(49) Baranov, A. V.; Rakovich, Y. P.; Donegan, J. F.; Perova, T. S.; Moore, R. A.; Talapin, D. V.; Rogach, A. L.; Masumoto, Y.; Nabiev, I. Effect of ZnS Shell Thickness on the Phonon Spectra in CdSe Quantum Dots. *Phys. Rev. B: Condens. Matter Mater. Phys.* **2003**, *68*, 165306.
(50) Beachell, H. C.; Taylor, H. A. The Thermal Decomposition of n-Butylamine. *J. Chem. Phys.* **1942**, *10*, 106−110.
(51) DiOrio, A. M.; Luo, X.; Lee, K. M.; Mather, P. T. A Functionally Graded Shape Memory Polymer. *Soft Matter* **2011**, *7*, 68−74.
(52) Droste, D. H.; Dibenedetto, A. T. The Glass Transition Temperature of Filled Polymers and its Effect on their Physical Properties. *J. Appl. Polym. Sci.* **1969**, *13*, 2149−2168.
(53) Chiou, B.-S.; Khan, S. A. Real-Time FTIR and in Situ Rheological Studies on the UV Curing Kinetics of Thiol-ene Polymers. *Macromolecules* **1997**, *30*, 7322−7328.
(54) Cramer, N. B.; Bowman, C. N. Kinetics of Thiol−Ene and Thiol−Acrylate Photopolymerizations with Real-Time Fourier Transform Infrared. *J. Polym. Sci., Part A: Polym. Chem.* **2001**, *39*, 3311−3319.
(55) White, T. J.; Natarajan, L. V.; Tondiglia, V. P.; Bunning, T. J.; Guymon, C. A. Polymerization Kinetics and Monomer Functionality Effects in Thiol−Ene Polymer Dispersed Liquid Crystals. *Macromolecules* **2007**, *40*, 1112−1120.

DOI: 10.1021/acsami.7b03366
ACS Appl. Mater. Interfaces 2017, 9, 17435−17448

(56) Hoyle, C. E.; Lee, T. Y.; Roper, T. Thiol–Enes: Chemistry of the Past with Promise for the Future. *J. Polym. Sci., Part A: Polym. Chem.* **2004**, *42*, 5301–5338.
(57) Lee, T. Y.; Bowman, C. N. The Effect of Functionalized Nanoparticles on Thiol–Ene Polymerization Kinetics. *Polymer* **2006**, *47*, 6057–6065.
(58) Chen, C.-J.; Chiang, R.-K.; Huang, C.-Y.; Lien, J.-Y.; Wang, S.-L. Thiol Treatment to Enhance Photoluminescence and Electroluminescence of CdSe/CdS Core-Shell Quantum Dots Prepared by Thermal Cycling of Single Source Precursors. *RSC Adv.* **2015**, *5*, 9819–9827.
(59) Zhou, H.; Li, Q.; Shin, J.; Hoyle, C. E. Effects of Monomer Functionality and Hydrogen Bonding on the Polymerization Kinetics and Properties of Thiol–Ene Networks. *Macromolecules* **2009**, *42*, 2994–2999.
(60) Pfeiffer, H. G.; Liebhafsky, H. A. The Origins of Beer's Law. *J. Chem. Educ.* **1951**, *28*, 123–125.
(61) Gao, X.; Cui, Y.; Levenson, R. M.; Chung, L. W. K.; Nie, S. In Vivo Cancer Targeting and Imaging with Semiconductor Quantum Dots. *Nat. Biotechnol.* **2004**, *22*, 969–976.
(62) Stutz, H.; Illers, K. H.; Mertes, J. A Generalized Theory for the Glass Transition Temperature of Crosslinked and Uncrosslinked Polymers. *J. Polym. Sci., Part B: Polym. Phys.* **1990**, *28*, 1483–1498.
(63) Krumova, M.; López, D.; Benavente, R.; Mijangos, C.; Pereña, J. M. Effect of Crosslinking on the Mechanical and Thermal Properties of Poly(vinyl alcohol). *Polymer* **2000**, *41*, 9265–9272.
(64) Ellison, C. J.; Torkelson, J. M. The Distribution of Glass-Transition Temperatures in Nanoscopically Confined Glass Formers. *Nat. Mater.* **2003**, *2*, 695–700.
(65) Ellison, C. J.; Torkelson, J. M. Sensing the Glass Transition in Thin and Ultrathin Polymer Films via Fluorescence Probes and Labels. *J. Polym. Sci., Part B: Polym. Phys.* **2002**, *40*, 2745–2758.
(66) Forrest, J. A.; Dalnoki-Veress, K.; Dutcher, J. R. Interface and Chain Confinement Effects on the Glass Transition Temperature of Thin Polymer Films. *Phys. Rev. E: Stat. Phys., Plasmas, Fluids, Relat. Interdiscip. Top.* **1997**, *56*, 5705–5716.
(67) Bansal, A.; Yang, H.; Li, C.; Cho, K.; Benicewicz, B. C.; Kumar, S. K.; Schadler, L. S. Quantitative Equivalence between Polymer Nanocomposites and Thin Polymer Films. *Nat. Mater.* **2005**, *4*, 693–698.
(68) Demir, M. M.; Castignolles, P.; Akbey, U.; Wegner, G. In-situ Bulk Polymerization of Dilute Particle/MMA Dispersions. *Macromolecules* **2007**, *40*, 4190–4198.
(69) Lecamp, L.; Youssef, B.; Bunel, C.; Lebaudy, P. Photoinitiated Polymerization of a Dimethacrylate Oligomer: 1. Influence of Photoinitiator Concentration, Temperature and Light Intensity. *Polymer* **1997**, *38*, 6089–6096.
(70) Jacobine, A. F. *Radiat. Curing Polym. Sci. Technol.* **1993**, *3*, 219–268.
(71) Timoshenko, S.; Woinowsky-Krieger, S.; Woinowsky-Krieger, S. *Theory of Plates and Shells*; McGraw-Hill: New York, 1959; Vol. 2.
(72) Jiang, C.; Markutsya, S.; Pikus, Y.; Tsukruk, V. V. Freely Suspended Nanocomposite Membranes as Highly-Sensitive Sensors. *Nat. Mater.* **2004**, *3*, 721–728.
(73) Markutsya, S.; Jiang, C.; Pikus, Y.; Tsukruk, V. V. Free-standing Multilayered Nanomembranes: Testing Micromechanical Properties. *Adv. Funct. Mater.* **2005**, *15*, 771–780.
(74) Kim, S.; Xiong, R.; Tsukruk, V. V. Probing Flexural Properties of Cellulose Nanocrystal–Graphene Nanomembranes with Force Spectroscopy and Bulging Test. *Langmuir* **2016**, *32*, 5383–5393.
(75) Gauthier, M. A.; Luo, J.; Calvet, D.; Ni, C.; Zhu, X. X.; Garon, M.; Buschmann, M. D. Degree of Crosslinking and Mechanical Properties of Crosslinked Poly(vinyl alcohol) Beads for use in Solid-Phase Organic Synthesis. *Polymer* **2004**, *45*, 8201–8210.
(76) Xia, Y.; Whitesides, G. M. Soft Lithography. *Angew. Chem., Int. Ed.* **1998**, *37*, 550–575.
(77) Ko, H. H.; Jiang, C. Y.; Tsukruk, V. V. Encapsulating Nanoparticle Arrays into Layer-by-Layer Multilayers by Capillary Transfer Lithography. *Chem. Mater.* **2005**, *17*, 5489–5497.
(78) Young, S. L.; Gupta, M.; Hanske, C.; Fery, A.; Scheibel, T.; Tsukruk, V. V. Utilizing Conformational Changes for Patterning Thin Films of Recombinant Spider Silk Proteins. *Biomacromolecules* **2012**, *13*, 3189–3199.
(79) Kuo, C.-Y.; Su, M.-S.; Ku, C.-S.; Wang, S.-M.; Lee, H.-Y.; Wei, K.-H. Ligands affect the crystal structure and photovoltaic performance of thin films of PbSe quantum dots. *J. Mater. Chem.* **2011**, *21*, 11605–11612.
(80) Kharlampieva, E.; Kozlovskaya, V.; Zavgorodnya, O.; Lilly, G. D.; Kotov, N. A.; Tsukruk, V. V. pH-Responsive Photoluminescent LbL Hydrogels with Confined Quantum Dots. *Soft Matter* **2010**, *6*, 800–807.
(81) Cook, S. M.; Schäffer, T. E.; Chynoweth, K. M.; Wigton, M.; Simmonds, R. W.; Lang, K. M. Practical Implementation of Dynamic Methods for Measuring Atomic Force Microscope Cantilever Spring Constants. *Nanotechnology* **2006**, *17*, 2135–2145.
(82) Würth, C.; Grabolle, M.; Pauli, J.; Spieles, M.; Resch-Genger, U. Relative and Absolute Determination of Fluorescence Quantum Yields of Transparent Samples. *Nat. Protoc.* **2013**, *8*, 1535–1550.

DOI: 10.1021/acsami.7b03366
ACS Appl. Mater. Interfaces 2017, 9, 17435–17448